Scaling and Numerical Model Evaluation of Snow-Cover Effects on the Generation and Modification of Daytime Mesoscale Circulations

M. SEGAL,* J. R. GARRATT,** R. A. PIELKE† AND Z. YE@

*Department of Physics and Astronomy, University of Kansas, Lawrence, Kansas
**CSIRO Division of Atmospheric Research, Mordialloc, Victoria, Australia
†Department of Atmospheric Science, Colorado State University, Fort Collins, Colorado
@Institute of Atmospheric Physics, Academia Sinica, Beijing, China

(Manuscript received 21 March 1990, in final form 16 October 1990)

ABSTRACT

Consideration of the sensible heat flux characteristics over a snow surface suggests a significant diminution in the magitude of the flux, compared to that over a snow-free surface under the same environmental conditions. Consequently, the existence of snow-covered mesoscale areas adjacent to snow-free areas produces horizontal thermal gradients in the lower atmosphere during the daytime, possibly resulting in a "snow breeze." In addition, suppression of the daytime thermally induced upslope flow over snow-covered slopes is likely to occur. The present paper provides scaling and modeling evaluations of these situations, with quantification of the generated and modified circulations. These evaluations suggest that under ideal situations involved with uniform snow cover over large areas, particularly in late winter and early spring, a noticeable "snow breeze" is likely to develop. Additionally, suppression of the daytime thermally induced upslope flow is significant and may even result in a daytime drainage flow. The effects of bare ground patchiness in the snow cover on these circulations are also explored, both for flat terrain and slope-flow situations. A patchiness fraction greater than ~0.5 is found to result in a noticeably reduced snow-breeze circulation, while a patchiness fraction of only ~0.1 caused the simulated daytime drainage flow over slopes to be reversed.

1. Introduction

Snow-covered ground is common as a temporary or long-term feature during the winter (and possibly fall and spring) in the mid-latitudes of the Northern Hemisphere. With the presence of elevated slopes, snow cover at this time of the year tends to occur in well-defined temporal and spatial patterns and, on many occasions, is limited to mesoscale domains. However, only a few studies (observationally oriented) have reported on snow-cover effects related to mesoscale atmospheric processes.

Any modeling investigation of lower atmospheric processes over snow-covered ground should ideally consider a two-way interactive snow–atmosphere system. For example, slab snow-layer formulations based on such a system have been introduced in general circulation models (e.g., Washington and Parkinson 1986; Dickenson et al. 1986), in order to resolve adequately the impact of the large snow-covered areas of the high latitudes on the general circulation. However, research attention given to the impact of snow-covered ground on circulations of smaller horizontal scale has been lacking. As will be discussed in section 3, snow-covered ground is associated with major modifications to the surface thermal fluxes and, therefore, on thermally forced circulations of mesoβ scale (i.e., with a horizontal scale ~ 20–200 km, henceforth termed mesoscale circulations). Such circulations include daytime thermally induced upslope flows.

The sporadic nature of snowfall in many geographical locations may result in a sharp transition from snow-covered ground to bare ground (e.g., Bluestein 1982; Schlatter et al. 1983; Cramer 1988; Segal et al. 1991a), and such patterns or discontinuities can be readily identified under clear sky conditions from visible and IR satellite images. They are likely to be associated with a corresponding horizontal thermal gradient and thermally induced circulation similar to a sea breeze—e.g., as implied in the observations along the Front Range of Colorado by Johnson et al. (1984), and indicated by Cramer (1988) and Segal et al. (1991a). Following Johnson et al. (1984), this type of circulation, which unlike the sea breeze, has not been widely investigated, is termed in the present study, a "snow breeze". A snow breeze is related to the group of nonclassical mesoscale circulations (NCMC) forced by differential terrain sensible heat fluxes. The contrast of snow-covered ground to snow-free ground is also common along mountain slopes during the seasonal melting period, with snow-free lower slopes and snow-covered elevated areas. Thus, a coupling of the slope

Corresponding author address: Moti Segal, University of Kansas, Dept. of Physics & Astronomy, 1082 Malott Hall, Lawrence, KS 66045.

snow breeze and the thermally induced upslope flow may generate, on such occasions, complex mesoscale circulations.

The reduction of the surface sensible heat fluxes during the daytime in the presence of snow cover leads to a suppression of the daytime development of the upslope circulation or even to a generation of a drainage flow (e.g., Ohata et al. 1981, for a small domain). Additional observational evaluations of this situation in a mesoscale domain are provided in Cramer (1988).

The impact of snow cover on mesoscale circulations as outlined above has been only little investigated through observational studies, yet may have important implications related to local weather prediction (mostly in the spring), and to air-pollution dispersion conditions. On the other hand, apparently no theoretical study has been carried out to quantify the snow-cover effect on those circulations. It is the purpose of the present study to provide initial scaling and numerical modeling evaluations of this impact. The study includes a summary of relevant snow-cover physics and a description of the snow-cover parameterization implemented in the atmospheric model adopted here (section 2). Model evaluations of the thermal forcing over snow are provided in section 3. Scale analysis, evaluating the impact of uniform and nonuniform snow cover on the induced circulations, is given in section 4. Illustrative numerical model simulations for a generic range of real-world situations are described in section 5.

2. Snow–atmosphere interactive model

One of the objectives of the present study is the introduction of a multilevel, interactive snow layer into the mesoscale model described by Mahrer and Pielke (1977) and McNider and Pielke (1981). Early studies of snow-layer physical processes (e.g., by Schlatter 1972; Anderson 1976) used noninteractive, multilevel snow-layer models with the surface-layer meteorological parameters either prescribed or obtained from surface observations. Later, Halberstam and Melendez (1979) developed a one-dimensional atmospheric boundary layer (ABL)–snow interactive numerical model for the study of the impact of snow cover on the ABL. In the present study, the snow-layer formulation has similarities to that of Anderson (1976) and of Halberstam and Melendez (1979), although some refinements pertinent to the present study have been included. A general discussion and description of the snow formulation is given below (note that SI units are used throughout).

a. Albedo

Snow albedo is dependent on several physical properties of the snow, including the grain size, snow liquid-water content, and amount of compaction. Some investigators (e.g., Anderson 1976) suggested, therefore, the use of a functional relation between the albedo and the density of the snow. The albedo of snow in the visible wavelength may be as high as 0.95 for fresh and deep snow, reducing with aging or melting. Typical values of snow albedo and its wavelength dependence, as reported by various investigators, have been reviewed by Mellor (1977), while an updated observational evaluation of the snow spectral albedo can be found in Wiscombe and Warren (1980). The snow albedo, mostly for fresh snow, is also somewhat dependent on sun zenith angles (with a smaller albedo around noon as compared to the morning and afternoon hours). On the time scale of the daytime mesoscale circulations studied here ($\sim$ several hours), the snow-albedo changes resulting from changes in the physical properties of the snow can be assumed, in general, to be insignificant. A simplified version of the relations suggested by Wiscombe and Warren (1980) and Dickenson et al. (1986) was adopted, giving the snow albedo a_s as

$$a_s = 0.5(a_{vo} + a_{io}) + 0.32f(\theta_z) \tag{1}$$

where a_{vo} (=0.95) is the albedo for a solar radiation wavelength ≤ 0.7 μm and a_{io} (=0.65) for a solar radiation wavelength > 0.7 μm. The stated values of a_{vo} and a_{io} are typical for fresh snow and zenith angles of less than 60°. Consideration of the effect of zenith angle, θ_z, on the albedo is expressed through the function:

$$f(\theta_z) = \frac{1}{b}\left(\frac{b+1}{(1+2b\cos\theta_z)} - 1\right) \tag{2}$$

with $b = 2$ and $f(\theta_z) = 0$ if $\cos\theta_z > 0.5$; also for $\theta_z > 80°$, the constraint $f(\theta_z) = f(\theta_z = 80°)$, was adopted. The increase in the downward solar radiation flux over a snow surface, due to multiple scattering between the surface and the atmosphere, is included (following Atwater and Ball 1978) as a multiplicative factor $(1 - 0.0685a_s)^{-1}$.

b. Surface roughness

The surface roughness of a uniform snow cover over flat ground is on the order of 10^{-4} m (e.g., Hicks and Martin 1972; Oke 1987). Several studies (e.g., Tabler 1980; Joffre 1982; Chamberlain 1983) suggest an analogy with rough flow over water surfaces, when the surface is affected by moderate to high winds, in which z_o is given by (e.g., Charnock 1955):

$$z_o = \alpha g^{-1} u_*^2. \tag{3}$$

Here α is a constant [Chamberlain (1983) suggested a value of 0.016, close to that given by Tabler (1980) and to the value appropriate for flow over the sea surface], u_* is the friction velocity, and g is the gravity acceleration. For light winds, z_o, given by Eq. (3), would be replaced by a constant value of $\approx 10^{-4}$ m.

When the snow-surface height varies, e.g., because of a canopy-covered ground (e.g., when bushes or forests are completely covered by snow) or a nonuniform snow depth results from melting, the surface roughness will be strongly related to these surface variations and may typically reach several centimeters. When the terrain under consideration consists of urban areas or forest patches, for example, the surface roughness will be related to the roughness of the main obstacles.

c. Thermal heat balance over snow surface

The heat balance equation at the snow surface is given below, where the sign convention is used that nonradiative fluxes are positive away from the surface, and radiative fluxes are positive towards the surface, —viz.

$$R_L + r(1 - a_s)R_S - H_s - E_s - K\frac{\partial T_s}{\partial z}\bigg|_S - \epsilon_s\sigma T_{s_o}^4 = 0 \quad (4)$$

with

$$K = \kappa_e + \kappa_s, \quad (5)$$

where

- E_s latent heat flux at the snow surface
- H_s sensible heat flux at the snow surface
- κ_e coefficient for heat conductivity in snow
- κ_s coefficient for heat transfer by sublimation in the snow layer
- R_L incoming long wave radiation at the snow surface
- R_S incoming global solar radiation at the snow surface (the sum of the direct and diffuse radiation)
- σ Stefan-Boltzman constant
- ϵ_s snow emissivity ($\epsilon_s \approx 1$ for fresh snow)
- r efficiency coefficient for absorption of solar radiation at the snow surface ($r = 0$: all nonreflected solar radiation penetrates into the snow layer; $r = 1$: all nonreflected solar radiation absorbed at the snow surface; in the present study an intermediate value of $r = 0.5$ was adopted)
- T_s snow temperature
- T_{so} snow surface temperature

The snow temperature, T_s, is limited, obviously, by the constraint $T_s \leq 273$ K.

Using the sample of observational studies presented in Anderson (1976), κ_e, was approximated, with a dependence on the snow density ρ_s, by the relation:

$$\kappa_e = 417e^{(7.013\rho_s - 9.721)}. \quad (6)$$

Following Anderson (1976) and Yen (1981) an equivalent thermal conductivity coefficient, κ_s, for heat transferred by sublimation (as a result of temperature gradients within the snow-layer), was expressed to a first order of approximation as

$$\kappa_s = L_s D_e f', \quad (7)$$

where

$$f' = \frac{e_i}{R_w T^2}\left[\frac{L_s}{R_w T_s} - 1\right] \quad (8)$$

and

$$e_i = 3.5558 \cdot 10^{12} \exp\left(-\frac{L_s}{R_w T_s}\right) \quad (9)$$

with

- D_e effective diffusion coefficient for water vapor in snow; following Anderson (1976) a representative value, $D_e = 0.65\ 10^{-4}$ m^2 s^{-1}, was assumed
- e_i saturation vapor pressure over ice (Pa)
- R_w gas constant for water vapor
- L_s latent heat of ice sublimation.

In the above, both κ_e and κ_s are in units of J m^{-1} s^{-1} K^{-1}.

d. Temperature stratification within the snow-layer

The temperature, T_s, within the snow layer is predicted by the equation:

$$C_i\rho_s\frac{\partial T_s}{\partial t} = \frac{\partial}{\partial z}\left(K\frac{\partial T_s}{\partial z}\right) + \eta(1 - r)(1 - a_s)R_s e^{-\eta z} - Lm_f, \quad (10)$$

where

- C_i specific heat of ice
- L latent heat of ice melting
- m_f rate of melted snow amount per unit volume and unit time
- z depth below the snow surface
- η extinction coefficient for penetrating solar radiation.

The first term on the rhs of Eq. (10) takes into account the heat transfer by conduction and sublimation in the snow layer. The absorption of solar radiation in the snow-layer, as given by Beer's law, is represented by the second term on the rhs of Eq. (10), and depends mostly on the snow density. The extinction coefficient η (in units of m^{-1}) is related to the snow density, following Anderson (1976), and is approximated as

$$\eta = 200\rho_s \quad \text{for} \quad \rho_s \leq 0.2$$
$$\eta = 40 - 66.7(\rho_s - 0.2) \quad \text{for} \quad \rho_s > 0.2. \quad (11)$$

Snow melting due to absorption of solar radiation or conduction of heat from warmed soil is represented by the fusion term, Lm_f. From a computational point

of view, when the snow temperature at any level is computed to be above 273 K, the computed temperature excess above this value is translated into the rate of snow melt m_f, necessary to maintain the temperature at 273 K. It is assumed that the water percolates to the bottom of the layer.

3. Factors affecting the surface sensible heat flux over snow cover

In the present study, the surface sensible heat flux, H_s, over snow is the main forcing related to the intensity of the simulated thermal circulations. In this section we present extensive conceptual and model evaluation of its characteristics for a variety of situations. Elaborations relating to the impact of H_s characteristics on the studied circulations are given in sections 4 and 5.

a. General evaluations of sensible heat fluxes

1) EFFECTS OF AIR TEMPERATURE AND SNOW ALBEDO

The magnitude of the horizontal gradient of sensible heat flux across a snow–bare soil boundary determines the intensity of the snow-breeze circulation as scaled later through Eq. (13). In ideal cases of uniform fresh and deep snow, $-50 \leqslant H_s \leqslant 50$ W m^{-2} (e.g., Hicks and Martin 1972; Granger and Male 1978). Extreme negative values of H_s are likely with strong warm flows (e.g., chinook winds, passage of warm fronts), while extreme positive values of H_s will occur with strong cold air flows (e.g., arctic flows, passage of cold fronts). In such situations, McKay and Thurtell (1978) computed (based on measurements) that $|H_s| > 50$ W m^{-2} on some occasions. Both of these extreme situations, however, are not pertinent in the current study because they are associated with strong background flows. In contrast, the values of sensible heat flux, H_s, over dry soil on sunny days, and on synoptically unperturbed days, is usually in the range 100–200 W m^{-2} during midwinter (e.g., Hicks 1981 and Table 2 in this paper). Obviously, the magnitude of H_s over land is closely related to the intensity of solar radiation, and so, for a given surface wetness, is highly dependent on the time of the year and latitude. Therefore, it is suggested that most intense snow breezes are likely to occur following fall and spring snow events in the southern mid-latitudes (Northern Hemisphere).

While the bulk evaluation of H_s is sufficient for scaling of the snow breeze under fresh snow cover (see section 4), it has to be evaluated in a more refined manner under less ideal situations, and particularly when thermally induced slope flows are considered.

Figure 1 provides an illustrative model evaluation of the impact of the background temperature, snow albedo, and snow surface roughness, on the 1200 LST values of H_s, assuming midwinter (21 December) and early spring (21 March) solar radiation conditions at

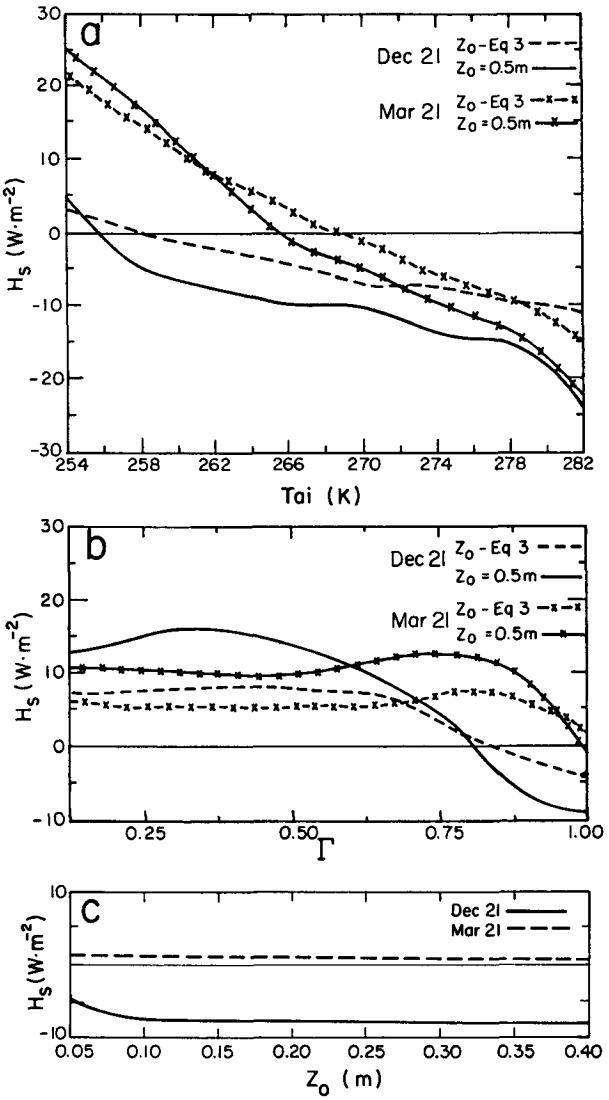

FIG. 1. One-dimensional model simulations evaluating the sensitivity of H_s at noon to changes in: (a) T_{ai}—the initial near-surface air temperature; (b) snow albedo: Γ is the fraction of fresh snow albedo; and (c) z_o—the surface roughness length.

a latitude of 40°N. The input parameters and other general simulation details are given in Table 1. The simulations were initialized by a geostrophic wind of 5 m s^{-1}, atmospheric potential temperature lapse rate $\partial\theta/\partial z = 0.0035$ K m^{-1}. Figure 1a presents the impact of the initial background temperature with a range of 254–282 K in near-surface temperatures T_{ai} (and therefore a corresponding range of temperature throughout the atmosphere). In both cases, the change in surface roughness from that derived by Eq. (3) to that of the extreme situation of a snow-covered tall canopy ($z_0 = 0.5$ m), does not produce significant variations in H_s. For the 21 March case, in which surface temperatures tended to be higher than for 21 December (due to larger solar radiation fluxes), H_s values in the

TABLE 1. Input parameters and initial profiles in the control model simulations (modifications in specific simulations are indicated in the text).

Soil	
Soil diffusivity	3×10^{-7} m^2 s^{-1}
Soil density	1.5 kg m^{-3}
Soil albedo	0.2
Soil moisture availability, m	0.05
Surface roughness	0.04 m
Δz in the soil layer	0.04 m
Snow	
Snow density (ρ_s)	0.2 kg m^{-3}
Snow surface solar radiation absorption efficiency (r)	0.5
Surface roughness	As given in Eq. (3) or as stated
Snow layer depth	0.24 m
Δz in the snow layer	0.003 m; 90 levels
Canopy	
Albedo	0.1
Surface roughness	0.5 m
Leaf Area Index	7
Canopy shielding factor	1
General	
Latitude	40°N
Simulated days	21 December and 21 March
Commencement of simulations	0800 LST
Horizontal grid interval	3 km
Time step	30 s
Model levels in the lower atmosphere	23 levels with variable spacing, top at 15 km
Initial near surface temperature	266 K (21 December); 271 K (21 March)
Initial vertical profile θ:	$\partial\theta/\partial z$ = 0.24 K m^{-1} near-surface, gradually changing to $\partial\theta/\partial z$ = 0.016 at 150 m; $\partial\theta/\partial z$ = 0.0035 K m^{-1} above 150 m
Initial specific humidity vertical profile	66% relative humidity

cold air environment ($T_{ai} < 266$ K) are larger. When the initial atmospheric temperature increases, computed H_s values reach -10 to -25 W m^{-2} for a near-surface air temperature of $T_{ai} = 282$ K.

As snow ages, snow-surface albedo may be lower than the values adopted in this study [i.e., as based on Eqs. (1)–(2)]. Figure 1b provides the noon-hour values of H_s assuming reduction factors, Γ, from the snow-albedo value a_s used in the regular simulations. When the albedo is relatively low, the snow-surface temperature reaches its maximum possible value of 273 K, and only small variations in H_s are found in this range of modified albedo. In this case, the relatively warm snow surface (resulting from increased absorption of solar radiation), in comparison to the cooler near-surface air temperature, results in a positive sensible heat flux (i.e., into the atmosphere). Decreases in the value of H_s, and reversal of its sign, are found for the high albedo values. Additional evaluations of H_s over snow are given in Segal et al. (1991b).

2) ESTIMATION OF THE EFFECT OF SNOW-SURFACE ROUGHNESS

Over uniform flat and fresh snow cover, the aerodynamic surface roughness, z_0, is small (on the order of $\leq 10^{-4}$ m) when the wind speed is light, and is given by Eq. (3) with relatively strong background winds. However, when the snow surface comprises noticeable variations (e.g., a relatively thin snow layer over ploughed fields; variations in snow depth due to non-uniform melting; and mostly when tall grass, bushes or trees are covered by snow), the surface roughness may increase considerably (suggested values are in the range $\sim$ 0.01 to $\sim$0.5 m). Figure 1c provides an illustration, based on 1-D model simulations, of the effect of variations of z_0 on H_s as simulated at 1200 LST. For the two presented days, the sensitivity of H_s to variations of z_0 (in the range 0.05–0.4 m) is small, mainly due to (i) the relatively light near-surface wind speed ($\sim$2 m s^{-1}) computed in the simulations and (ii) the rapid thermal adjustment of the snow layer to heat exchange with the atmosphere due to the snow's low heat capacity and reduced thermal conductivity.

3) COMPARISONS WITH LONGWAVE FLUX DIVERGENCE EFFECTS

The net longwave radiative flux divergence (ΔLWR) within the lower atmosphere over snow cover is likely to affect its thermal structure. For the comparable situation of a nocturnal stable surface layer over bare ground, observed values of ΔLWR are rarely available. The observational study by Manins and Sawford (1979) implies similar values of ΔLWR to that of the sensible heat flux divergence, ΔH_s. Recently, in an observational study, Estournel et al. (1986) suggested that the ΔLWR thermal effect, within the nocturnal ABL, is smaller than that of ΔH_s. In contrast, numerical studies of the nocturnal boundary layer (e.g., Garratt and Brost 1981) emphasize the importance of the longwave fluxes and, generally, show comparable cooling rates due to ΔLWR and ΔH_s.

In order to evaluate the significance of daytime values of ΔLWR in the lower atmosphere over *snow cover*, selective vertical profiles of ΔLWR cooling/heating rates (based on the simulations described in Fig. 1a), are presented and compared with those related to cooling due to ΔH_s. The 21 December case (Fig. 2a) and the 21 March case (Fig. 2b) generally show similar features. For the stable ABL [i.e., near-surface temperature $T_{ai} = 274$ K (moderately stable) and of $T_{ai} = 282$ K (intensely stable], relatively strong cooling contributions result from ΔH_s, which are limited to a shallow near-surface layer. The cooling related to

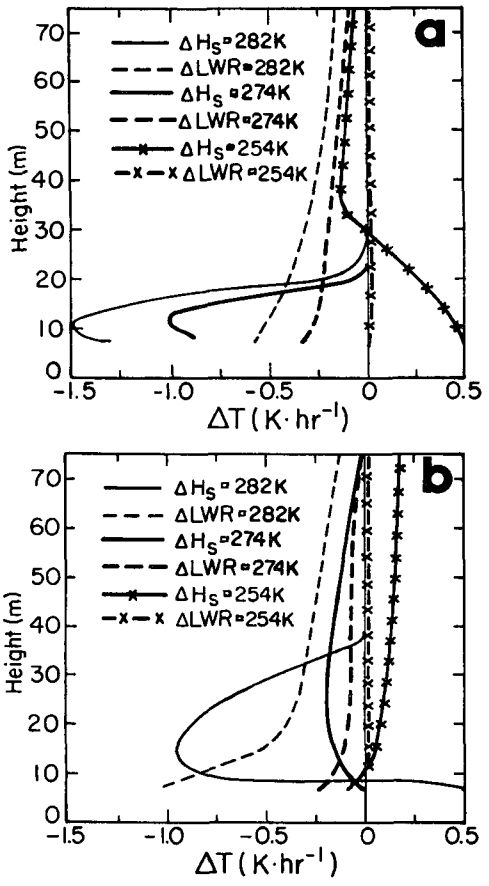

FIG. 2. Illustrative cooling/heating rate, ΔT, profiles within the lower atmosphere due to sensible heat flux divergence (ΔH_s) and longwave radiation flux divergence (ΔLWR). These are obtained from the simulations used to produce Fig. 1a with z_o based on Eq. (3); the initial near-surface temperature, T_{ai}, is indicated; (a) December 21 and (b) March 21.

ΔLWR extends through a deeper layer, gradually reducing with height. Overall, the height integrated cooling rates of ΔH_s and ΔLWR within the illustrated layer are about the same for the case of the intense stable ABL. For the moderately stable ABL, the cooling contribution by ΔH_s is somewhat larger. Similar features were simulated by McNider and Pielke (1981) and Garratt and Brost (1981) for the nocturnal ABL over bare ground. When an unstable surface layer is generated over the snow cover (i.e., due to advection of cold air, as illustrated by the 254 K initial near-surface temperature in Fig. 2), the warming contribution by ΔH_s (although quite small) is significantly large compared to ΔLWR.

In conclusion, it is suggested that the daytime ΔLWR cooling/heating contribution within the ABL over a snow cover is typically somewhat lower than that of ΔH_s. Thus, evaluations in the next sections will be made including H_s only; any effects of the additional cooling/heating involved with ΔLWR can be deduced, at least qualitatively, from Fig. 2.

b. Snow over forested area

1) CANOPY COATED BY SNOW

On some occasions, following snow storms over forested areas, canopies are almost completely covered by snow. The area can be viewed as a snow cover with a relatively large value of z_o. Figures 1a–c can be used to evaluate the values of H_s over snow covered canopy during sunny periods that follow such snowfall. As evaluated previously (subsection 3a.2), the impact of the increased surface roughness on the sensible heat flux, under low surface wind conditions and following an adjustment period, is quite small.

2) SNOW COVER BELOW CANOPY

On many occasions, within a relatively short period of time (i.e., several days), any snow accumulated on the canopy has mostly or completely melted or fallen to the ground. In the case of evergreen forests, the Leaf Area Index can be as large as 7 (e.g., Monteith 1976), while for deciduous forests (in fall) the Stem Area Index can approach a value of 2 (e.g., Dickinson et al. 1986), so the shielding of solar radiation, mostly below the evergreen canopy, may be significant. Since for most of the time winter evergreen forests do not transpire, it is suggested that a relatively large fraction of the available net radiation at the surface in areas affected by snow is converted into sensible heat flux. Detailed evaluations of the impact of evergreen canopies on the surface sensible heat flux and the ABL during the winter are provided, e.g., in Segal et al. (1989). Using the vegetation module of McCumber (1980) for (i) a canopy over a snow-free surface and (ii) a canopy over a snow surface, selective sensitivity simulations were performed to illustrate the impact on the exchange of sensible heat between the canopy and the atmosphere. Winter and early spring cases, where the surface was fully covered by a dense forest canopy (with a Leaf Area Index = 7 and a forest surface roughness, z_o = 0.5 m), were considered. The initial surface temperature below the canopy was the same in all cases, while a canopy shielding factor of one (i.e., fully covered area by canopy), is assumed. As can be deduced from Table 2, the existence of a snow cover below the canopy has

TABLE 2. H_s values (W m^{-2}) for a canopy surface (with and without snow cover below the canopy) and for snow-free soil (without canopy). Values of global solar radiation available at the surface are given in parenthesis. Computations based on 1-D model simulations for the indicated days and surface roughness heights.

	Canopy		Snow-free soil	
	Day		Day	
	21 Dec	21 Mar	21 Dec	21 Mar
Snow	244 (434)	466 (766)	168 (374)	350 (672)
No snow	251 (434)	482 (766)		

only a small effect on the exchange of sensible heat flux between the canopy and the atmosphere. Thus, it is suggested that, in general, a snow-free canopy (although snow cover may exist below the canopy) will be associated with a significant flux of sensible heat into the atmosphere on sunny winter days in mid-latitudes. Worth noting is that the sensible heat flux is larger for the canopy than for the snow-free soil, since for the latter, the albedo is higher and the subsequent heat transport into the subsoil is considerably larger.

c. *Bare soil patches/mixed areas*

The existence of bare soil patches, mostly when the snow is at the melting stage, as well as nonuniformity of the snow cover due to vegetation, urban areas, etc., are common on many occasions. Obviously, such heterogeneous cover should lead to an increase in the sensible heat flux over the area and to enhanced snow melting (e.g., Gray and O'Neil 1974). As a crude approximation, the sensible heat flux $\langle H_s \rangle$ for a unit area of nonuniform snow cover associated with uniformly distributed small snow-free patches is

$$\langle H_s \rangle = (1-f)H_s|_{\text{snow}} + fH_s|_{\text{snow free}}, \quad (12)$$

where f is the fraction of snow-free ground. Evaluation of the snow breeze and daytime thermal slope flows under these conditions are given in sections 4 and 5.

4. Scale analysis evaluations

In this section, we will focus on daytime situations associated with thermally induced flows forced by a snow-covered area adjacent to bare ground, or with thermally induced circulations along slopes. Sensitivity simulation results presented in previous sections provide input to some of the evaluations.

a. *Analytical evaluation of the circulation intensity*

1) SNOW BREEZE

For NCMCs involved with a snow–bare ground contrast the surface-induced line circulation provides an estimation for the intensity of the induced NCMC. Following Segal et al. (1988a), for example, the surface line circulation between point A located at the edge of the circulation over the snow and point B located at the edge of the circulation over the bare ground and at time t following sunrise, can be estimated by

$$\int_A^B u_s dl = \hat{K}_1 e^{-\hat{\alpha}t} \int_0^t \left[e^{\hat{\alpha}\tau} \int_0^\tau (H_s^A - H_s^B) d\tau' \right] d\tau \quad (13)$$

where

u_s surface flow component in the circulation direction
$\hat{K}_1$ constant—a product of physical constants
$\hat{\alpha}$ Rayleigh friction coefficient
H_s^A sensible heat flux over the snow area at A
H_s^B sensible heat flux over the snow-free area at B.

The sensible heat flux over the bare ground is the main forcing related to the intensity of the thermal circulations evaluated in the present study. This conclusion is readily derived from Eq. (13) and results presented in section 3, and it is consistent with that suggested by numerical model simulations of lake breezes (see Segal and Pielke 1985; Arritt 1987). In this section, we present an evaluation of the thermal forcing of circulations arising from differential snow cover.

Assume a uniform snow cover in a mesoscale region and air temperature above 273 K, as may occur frequently under sunny days with flow from low latitudes. In these cases, $H_s < 0$ over the snow. In this situation, the snow plays a role similar to that of a frozen lake (whose temperature ≤ 273 K), so that snow and frozen-lake breezes are expected to be of comparable intensity for the same environmental conditions. In contrast, with the snow cover in the mesoscale region replaced by a water body, air–water temperature differences may be close to zero, or even negative. Consequently, H_s will be smaller or even reversed in sign compared to that over snow surface, and the implied sea breeze of slightly less intensity than the potential snow breeze. Even when the snow surface is warmer than the air, based on previous evaluations (see section 3), the thermal difference between the snow and the land is not significantly affected and so the induced snow breeze will not be appreciably influenced. On many occasions, bare soil or vegetation patches in the snow-covered area occur, and as suggested in subsection 3c, the effective sensible heat flux over the snow can be approximated by a linear weighting [Eq. (12)], and thus the snow breeze is expected to decrease in intensity.

In order to evaluate the potential intensity of the mid-latitude snow breeze using Eq. (13), the surface sensible heat fluxes over bare ground, integrated from sunrise to midday, were approximated based on the relation:

$$\hat{H}_s = c \int_{\text{sunrise}}^{\text{noon}} (1-\hat{a}) R_S dt, \quad (14)$$

where R_S is the sum of the direct and the diffuse radiation (computed as outlined in Segal et al. 1988b), $\hat{a}$ is the bare ground albedo (assumed to be 0.2), and c is a proportionality scaling constant which, based on the numerical model simulations described in this paper (in sections 3 and 5), $c \approx 0.4$ over dry ground. The approximated values of $\hat{H}_s$ are given in Table 3. Over uniform snow it can be assumed (based on the evaluations in section 3) that $|\hat{H}_s|_{\text{snow}} \leq 0.1(|\hat{H}_s|_{\text{snow free}})$ where the ΔLWR cooling effect should not change the related thermal impact. Therefore, following Eq. (13), Table 3 provides an indication

TABLE 3. Estimated time integrated surface sensible heat fluxes, $\hat{H}_s$ ($\times 10^6$J), at noon at mid-latitude locations for various months (computed for the 21st day of the month following Segal et al., 1988b).

Latitude (°N)	Month											
	Jan	Feb	Mar	Apr	May	Jun	Jul	Aug	Sep	Oct	Nov	Dec
35	1.77	2.43	3.33	4.08	4.58	4.71	4.54	4.04	3.31	2.46	1.78	1.50
40	1.42	2.01	3.07	3.95	4.55	4.73	4.50	3.91	3.09	2.14	1.44	1.16
45	1.08	1.75	2.79	3.77	4.48	4.72	4.44	2.69	2.81	1.83	1.09	0.82

of the relative change of the snow breeze surface-line circulation intensity as functions of month and latitude. For example, the scaling suggests that at latitude 45° the winter (December) snow-breeze surface-line circulation intensity is only 22% of that of the spring (April) snow breeze. The midwinter snow-breeze surface-line circulation intensity at 35°N tends to be nearly double that at 45°N, although toward spring it tends to be similar at the various mid-latitude locations. The climatologically based $\hat{H}_s$ values for snow-free months provide input for scaling of the sea breeze in this period of the year. It is suggested that the summer (June) sea-breeze surface-line circulation intensity is ~3.1 times more intense as compared to a December snow breeze at 35°, and ~5.7 times more intense at 45°N. Comparing the June sea breeze to spring snow breeze (March) surface-line circulation suggests a factor of ~1.4 at 35°N and ~1.7 at 45°N.

When the snow cover is nonuniform due to small-scale bare soil patches or canopy, $\hat{H}_s$ computations based on Eq. (12) provide a first approximation for the modification in $\hat{H}_s$ over the snow cover. As mentioned above, $|\hat{H}_s|$ over uniform snow is negligible compared to that over adjacent bare ground. Therefore, when the fraction of snow-free patches, f (assumed to be uniformly spread within the snow area), exceeds some critical value, f_o, it is likely that the contribution of the snow-free patches to the areal averaged $\langle \hat{H}_s \rangle$ becomes more significant than the contribution from the snow surface. Thus, for a patchy snow cover, with $\hat{H}_s < 0$ over the snow surface, using Eq. (12), the value of the areal-averaged surface sensible heat flux $\langle \hat{H}_{s_p} \rangle$ should be given approximately by

$$\langle \hat{H}_{s_p} \rangle = (f - f_o)\hat{H}_s|_{\text{snow free}} \qquad (15)$$

where f_o can also be interpreted as the minimal area of snow-free patches in the snow-covered area needed to offset the negative sensible heat flux contribution from the snow. Based on Eq. (13), it is suggested that the reduction of the snow-breeze intensity with snow-free patches is by a factor $\Omega = 1 - f/(1 + f_o)$ compared to that associated with uniform snow cover. Assuming a warm day ($T_a > 273$ K), and thus a stable surface layer over the snow cover, based on the previously suggested scaling $|\hat{H}_s|_{\text{snow}} \leqslant 0.1\,|\hat{H}_s|_{\text{snow free}}$, yields $f_o \leqslant 0.1$. Therefore, if $f = 0.25$, then $\Omega = 0.77$, and for $f = 0.5$, $\Omega = 0.54$.

2) UPSLOPE FLOW

Based on the evaluations of H_s and ΔLWR presented in section 3, it is suggested that over a *uniformly snow-covered* slope, a daytime thermally induced downslope flow is likely to be generated in many cases. Comparing the values of H_s and ΔLWR computed over snow cover, as well as those involved with nocturnal drainage flows (e.g., see Table 1 in Ye et al. 1989) it is suggested that, occasionally, the two thermal components are of comparable intensity. The scaling presented in the previous subsection suggests that, for a uniform distribution of snow-free patches within the snow-covered area, a suppression of the daytime thermally induced downslope flow will result for $f_o \approx 0.1$. However, when the patches are large and isolated, downslope flows over the snow cover, perturbed by local upslope flow generated over the snow-free patches, are likely to be generated. In this case, areal suppression of the drainage flow will occur only for $f_o > 0.1$. The related value of f_o, in the last case, is determined by the configuration of the snow-free patches within the relevant area and their size.

5. Numerical model simulations

In the following subsection, a refined evaluation will be made through modeling in order to determine the effects of a range of parameters on the intensity of snow breezes, and on the thermally induced daytime upslope flows over snow-covered slopes. The simulations discussed here are for midwinter (21 December) and late season conditions (21 March) under clear skies. The purpose of the simulations is to explore a variety of situations with snow cover which are illustrative of real-world cases. Given the variability of the physical properties of snow and the generic nature of the simulations, the input parameters listed in Table 1 were chosen. Results are presented for 1400 LST when the circulations are near their peak intensity. The bare ground surface wetness is low with the surface moisture availability value, $m = 0.05$ (m is the ratio between the actual surface evaporation and potential evaporation).

a. Snow breeze

As evaluated in section 3, the magnitude of H_s and ΔLWR over snow is generally small, and comparable

under light synoptic flows to that over cold water bodies (e.g., see the nomogram for the derivation of H_s values over water surfaces in Kondo 1975). Thus, assuming a uniform and complete snow cover, it is anticipated that snow-breeze intensity similar to that of a sea breeze under winter conditions will result (worth noting is that sea-breeze-circulation characteristics in winter mid-latitudes are, in general, undocumented). In the following, simulations of snow breezes, mostly under uniform and extended snow-cover situations, are given, thus providing the upper limit to the circulation intensity. Selected vertical cross sections of the simulated horizontal flow (u component—perpendicular to the snow-bare ground boundary, and the corresponding v component; the v component is presented when it is noticeably large), the vertical velocity and the potential temperature as pertinent, are presented. A list of the simulations is provided in Table 4.

Snow-breeze characteristics for 21 December solar radiation conditions are shown in Fig. 3 (SB1). At 1400 LST the snow breeze u component reached a value of $\approx$4 m s^{-1}, while the breeze layer is relatively shallow ($\approx$600 m). The thermal stratification over the snow section is stabilized close to the surface, thus, it is not conducive to the development of a deep ABL. As a result the snow-breeze intensity is mostly affected by the amount of warming over the bare ground area, permitting a deep horizontal pressure gradient to develop between the snow-covered and bare ground areas, as suggested by the scaling presented in the previous section. The ABL peak depth over the snow-free ground is $\sim$1300 m based on the θ cross section. The vertical velocity associated with the snow breeze is small, $\approx$0.06 m s^{-1} for a horizontal grid resolution of 3 km.

Coupling of the snow breeze with the synoptic flow is shown in the next two cases. When a supportive synoptic flow (i.e., from snow towards the snow-free area) of 5 m s^{-1} is introduced (SB2) the snow breeze is seen only as a small perturbation to the synoptic flow, although it penetrates farther into the snow-free area compared to that presented in SB1 (Fig. 4a). A gradual change in the ABL depth is simulated over the snow-free area as a result of the advection of the cold air (originating over the snow) across the heated snow-free area (Fig. 4b). The significance of this ABL feature

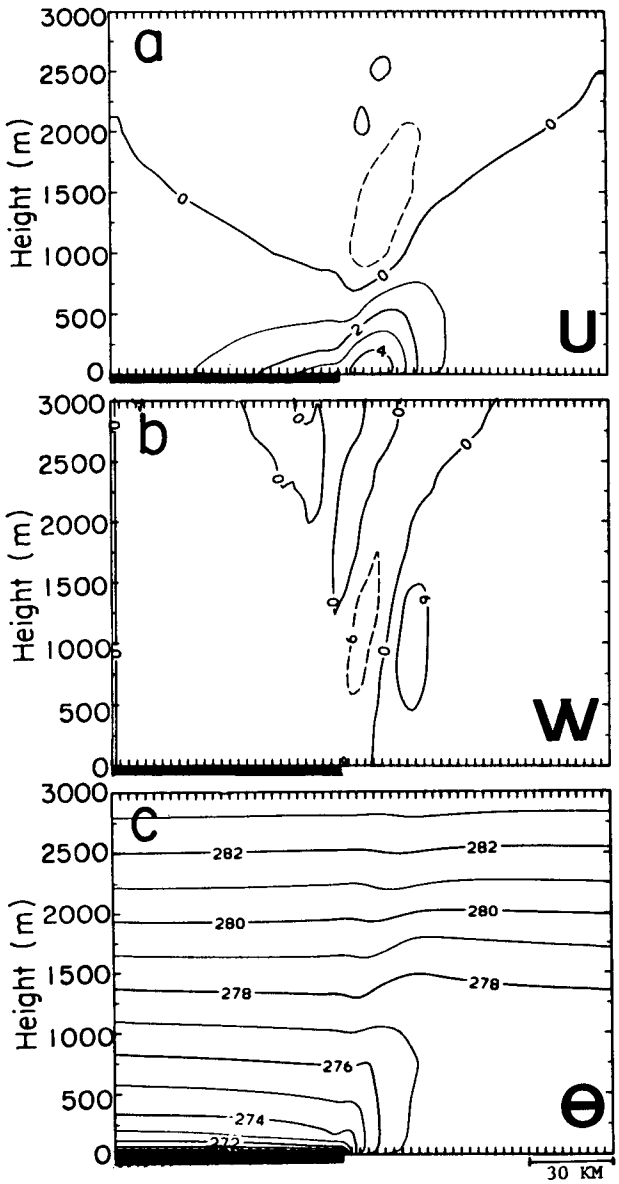

FIG. 3. Simulated snow-breeze features, at 1400 LST, in the domain vertical cross section for case SB1. (a) u component (m s^{-1}) (perpendicular to the snow–snow-free boundary; positive values—solid contours, indicate flow component from the snow to the snow-free area); (b) vertical velocity, w (cm s^{-1}) (upward motion—solid contours; downward motion—dashed contours; contour interval 6 cm s^{-1}); and (c) potential temperature, θ (K). The snow-covered area is indicated by the dark line along the abscissa.

TABLE 4. Brief description of the snow-breeze simulations (U_g—geostrophic wind normal to the snow boundary; and date).

Simulation	Description	Figure
SB1	U_g = 0, 21 December	3
SB2	U_g = 5 m s^{-1}, 21 December	4
SB3	U_g = −5 m s^{-1}, 21 December	5
SB4	U_g = 0, 21 March	6
SB5	U_g = 0, 21 March, m = 0.5	7
SB6	U_g = −5 m s^{-1}, 21 March	8
SB7	As SB4, with f = 0.25, 0.50, 0.75	9

can be evaluated and compared to the ABL features in SB1. The simulated vertical velocities are lower than in the previous case (not shown), since the snow-breeze front is weaker in the presence of a supportive synoptic flow. When the synoptic flow opposes the snow-breeze propagation (SB3), a shallow snow breeze is produced with a small u component over a portion of the snow area (Fig. 5a). Similar features (although for the sum-

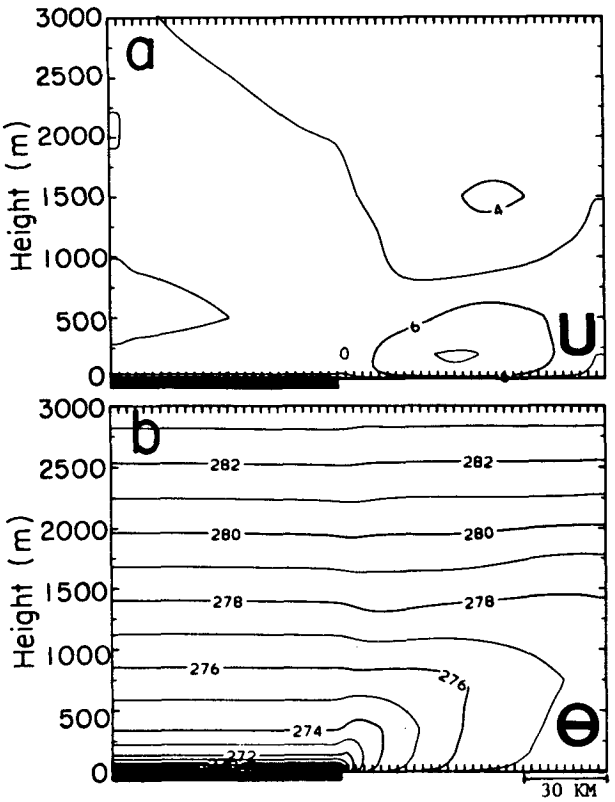

FIG. 4. Simulated snow-breeze features for case SB2. (a) u (m s^{-1}) component (m s^{-1}); and (b) potential temperature, θ (K).

mer period) have been found for sea breezes with opposing synoptic flow (e.g., Estoque 1962; Mahrer and Segal 1979). The coupling of the synoptic flow with the snow breeze leads to a noticeable convergence (Fig. 5b), with advection of relatively warm air from the bare ground area towards the snow resulting in the development of an intense inversion over the snow; Fig. 5c (compare with SB1, Fig. 3c).

The same snow-breeze simulations as above, except for 21 March, were also carried out. Figure 6 (Case SB4) presents the simulated field with no synoptic flow. The incoming solar radiation is close to a factor of ~2.6 larger than that on 21 December (see Table 3; 40°N), implying (as a first approximation) a similar increase in the time integrated surface sensible heat flux $\hat{H}_s$ and thus in the surface-line circulation. The intensity of the cross-boundary flow, u, reaches a peak of ~6 m s^{-1} (Fig. 6a) with some veering of the flow due to the Coriolis force (as revealed in the v component, Fig. 6b). The peak upward velocity was noticeably larger than in Case SB1 (Fig. 6c), reaching a value of 0.3 m s^{-1}. The bare ground ABL depth (as derived from Fig. 6d) increases by a factor of ~1.5 as compared to SB1, consistent with a change in $\hat{H}_s$ by a factor of 2.6 since the depth of the daytime convective ABL is proportional to $(\hat{H}_s)^{1/2}$. Noticeably, the warmer snow surface (273 K) results in a weaker surface tem-

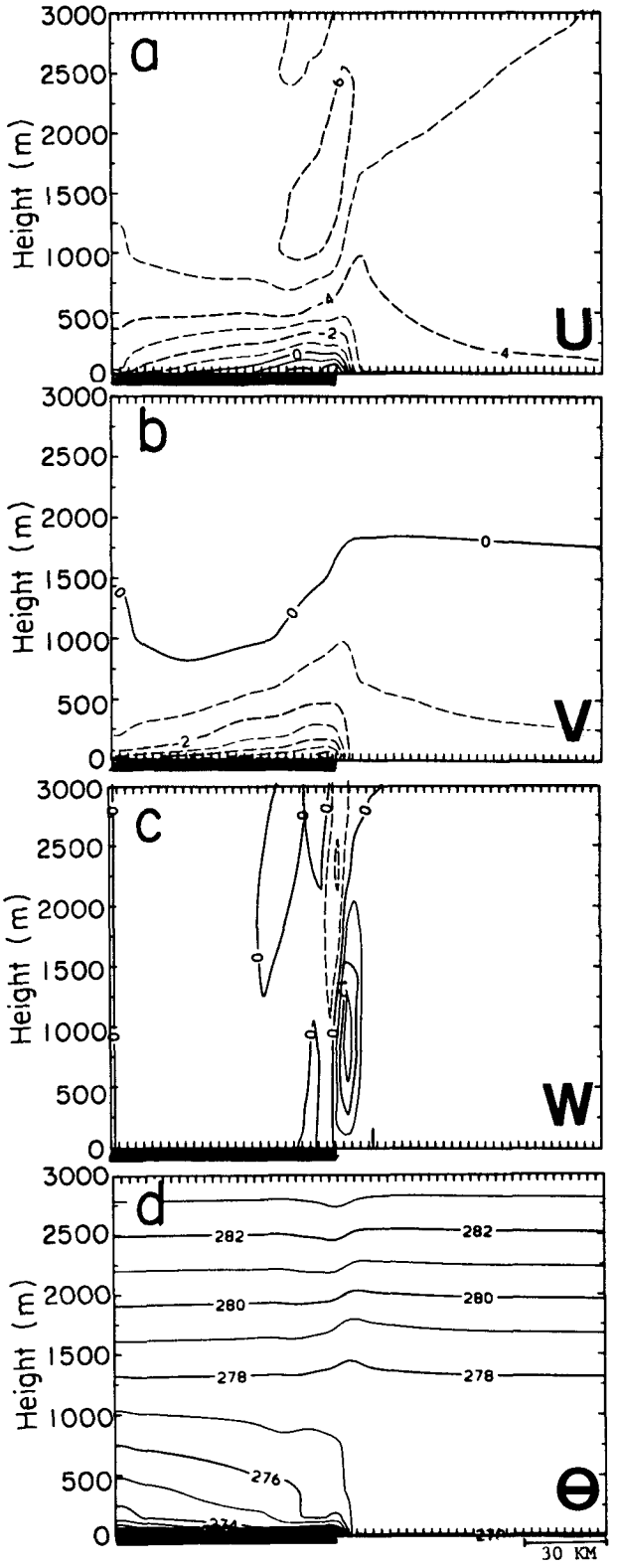

FIG. 5. Simulated snow-breeze features for case SB3. (a) u component (m s^{-1}); (b) v component (m s^{-1}) (parallel to the snow–snow-free boundary; negative values—dashed contours, indicate a flow component out of the figure); (c) vertical velocity (cm s^{-1}); and (d) potential temperature, θ (K).

perature inversion over the snow as compared to the December cases (Fig. 6d). On occasions of rapid melting of the snow cover, wet ground is likely to result in areas adjacent to the snow-cover area. Case SB5 reflects such a situation with a soil moisture availability of $m = 0.5$, resulting in some suppression of the thermally induced flow (Fig. 7a) as compared to the Case SB4 (Fig. 6a). The vertical velocity peak has decreased considerably (Fig. 7b), while the thermal stratification (not shown) is only slightly affected. The relatively low surface temperatures at this time of the year suggests a larger Bowen ratio than in the same situation with higher background temperatures; see evaluations in Segal et al. (1989). Thus, the relative impact of the wet surface is likely to be lower than in summer sea-breeze situations. In the supportive synoptic flow case (similar to case SB2; not shown) the existence of a snow-breeze perturbation to the flow was very noticeable compared to SB1. With an opposing synoptic flow (Fig. 8, Case SB6) the coupling with the snow breeze shifts the circulation toward the snow, with a convergence zone of depth ~ 500 m (Figs. 8a,b) and relatively large vertical velocities (Fig. 8c). The surface inversion is somewhat more pronounced when compared to SB4 (see Fig. 6), as a result of the advection of warm air towards the snow surface (Fig. 8d).

Figure 9 presents the u component of the snow breeze induced by a contrast of patchy snow and an adjacent snow-free area, for the background conditions used in Case SB4. The bare ground patches within the snow-covered area were assumed to be small in size and uniformly distributed (otherwise, assuming large nonuniform patches, secondary thermal circulations are likely to be generated between the patches and the surrounding snow). The surface-layer computations were carried out separately for the snow and the snow-free surfaces, where weighting of the sensible heat flux exchange with the atmosphere is used following Eq. (12). This method (or any other that does not involve an increased model horizontal grid resolution) provides only a first approximation of the net effect of the spatially variable surface on the area-averaged fluxes.

The reduction in the snow breeze when the bare ground fractional coverage increases from $f = 0.25$ (Fig. 9a) to 0.75 (Fig. 9c) is very noticeable, with a corresponding reduction in the peak u component from ~5 to 2 m s^{-1}, and a noticeable reduction in the horizontal extent of the circulation. It is worth noting that snow-free patches are typical of the melting stage following light snow fall and also may result from the redistribution of snow by strong winds. However, situations with uniform snow cover in relation to the snow breeze should not be seen as uncommon in the real world.

b. Slope simulations

Slope simulations were carried out with a topographic configuration which we describe as plain-

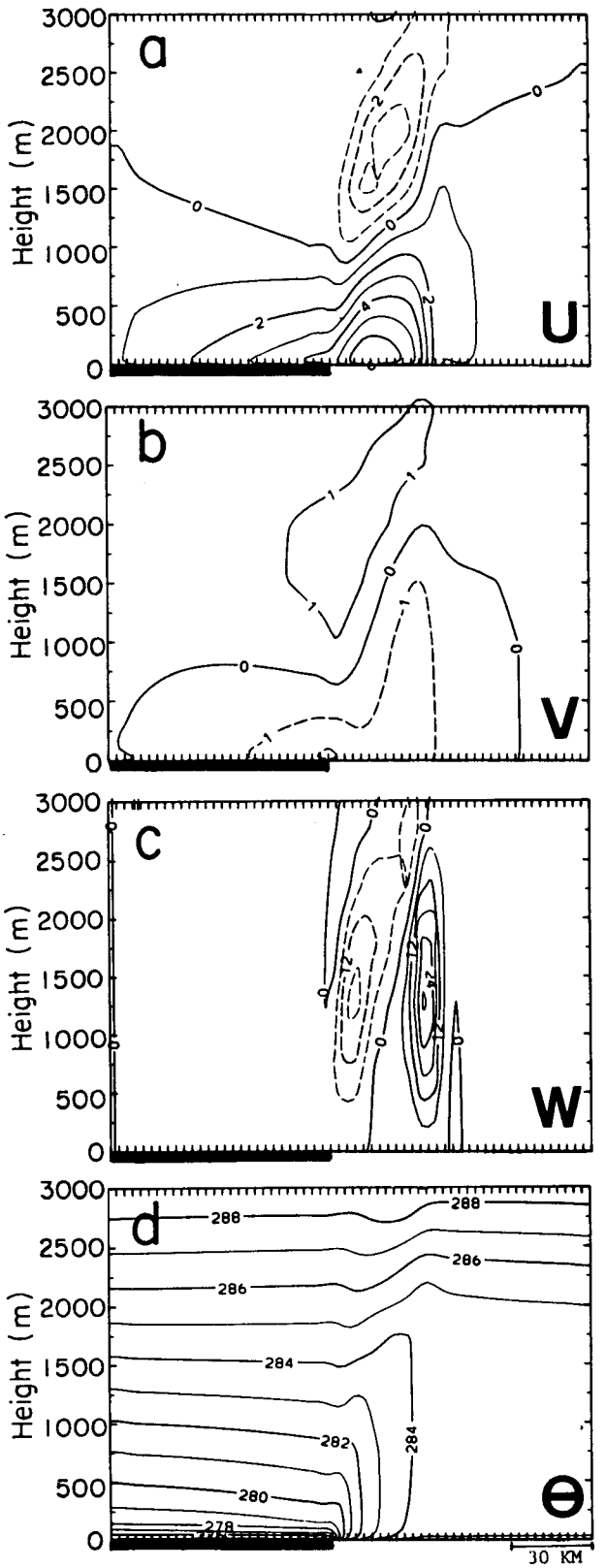

FIG. 6. Simulated snow-breeze features for case SB4. (a) u component (m s^{-1}); (b) v component (m s^{-1}); (c) vertical velocity (cm s^{-1}); and (d) potential temperature, θ (K).

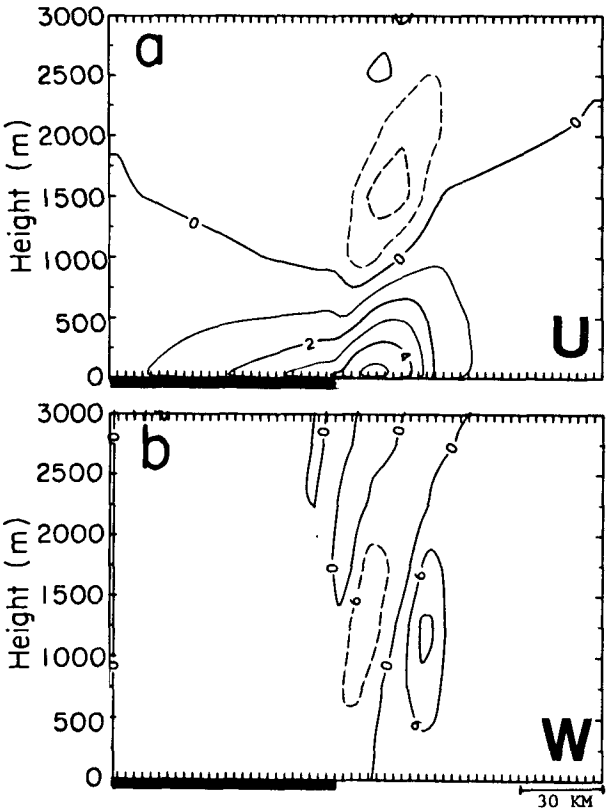

FIG. 7. Simulated snow-breeze features for case SB5. (a) u (m s^{-1}) component (m s^{-1}) and (b) vertical velocity, w (cm s^{-1}).

slope–plateau. Height of the plateau above the level ground (plain) was taken as either 400 or 800 m, with the slope extending over a 60 km distance (reflecting slope angles of $\alpha \approx 0.4°$ and $\alpha \approx 0.8°$, respectively). As in the earlier simulations, 21 December and 21 March were selected as representative days. Illustrative results at 1400 LST (a time at which the daytime thermally induced upslope flows are near their peak) are provided below. As in the previous section, vertical cross sections of various fields, are presented. A list of the simulations is presented in Table 5.

For midwinter and a snow-covered shallow slope (SL1; Fig. 10), a shallow drainage flow develops having light wind speeds ($u \approx 3$ m s^{-1}, $v = -2$ m s^{-1}; the development of a noticeable v component is attributed to the turning of the wind associated with reduced frictional effects) and a shallow surface temperature inversion. When this simulation is repeated, however, with lower background temperatures (Case SL2; the initial atmospheric potential temperature was decreased by 10 K), a suppression of the negative surface sensible heat flux in the morning hours, and a change in its sign later in the day (not shown) result in a significant reduction of the daytime downslope flow (Fig. 11a). Also noticeable is the resultant thermal desta-

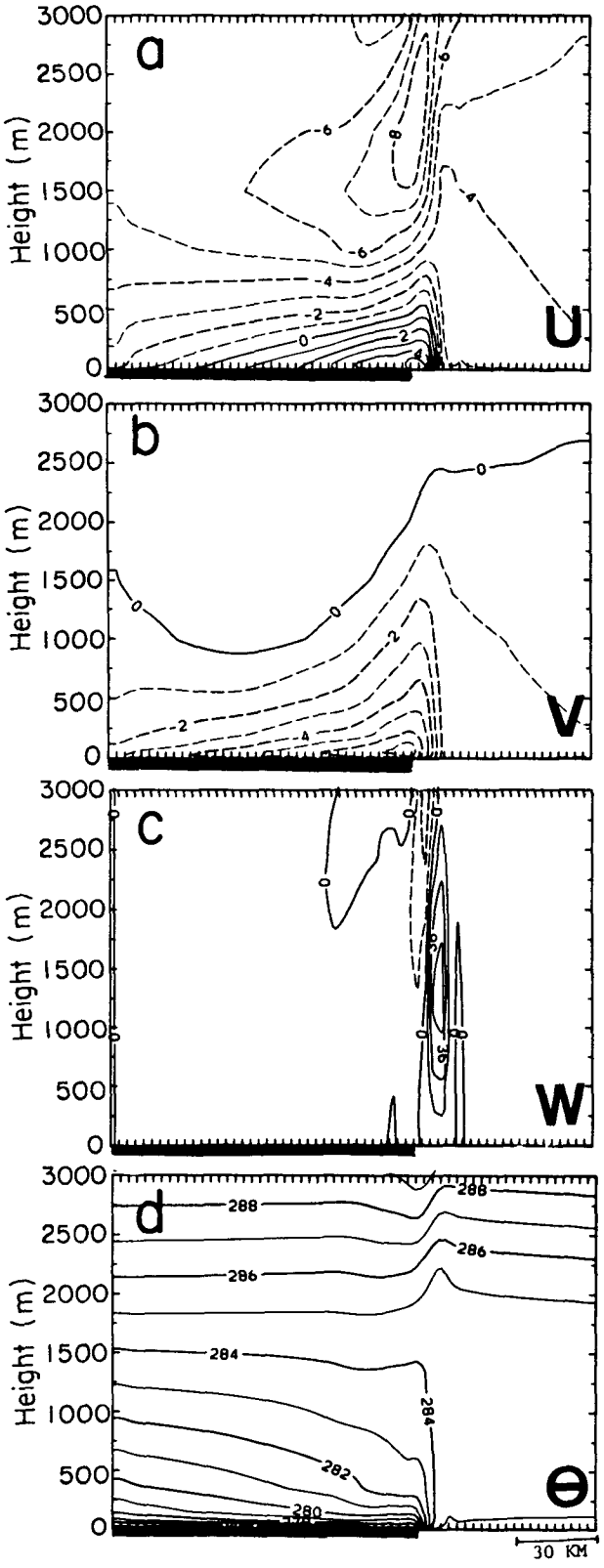

FIG. 8. Simulated snow-breeze features for case SB6. (a) u component (m s^{-1}); (b) v component (m s^{-1}); (c) vertical velocity, w (cm s^{-1}); and (d) potential temperature, θ (K).

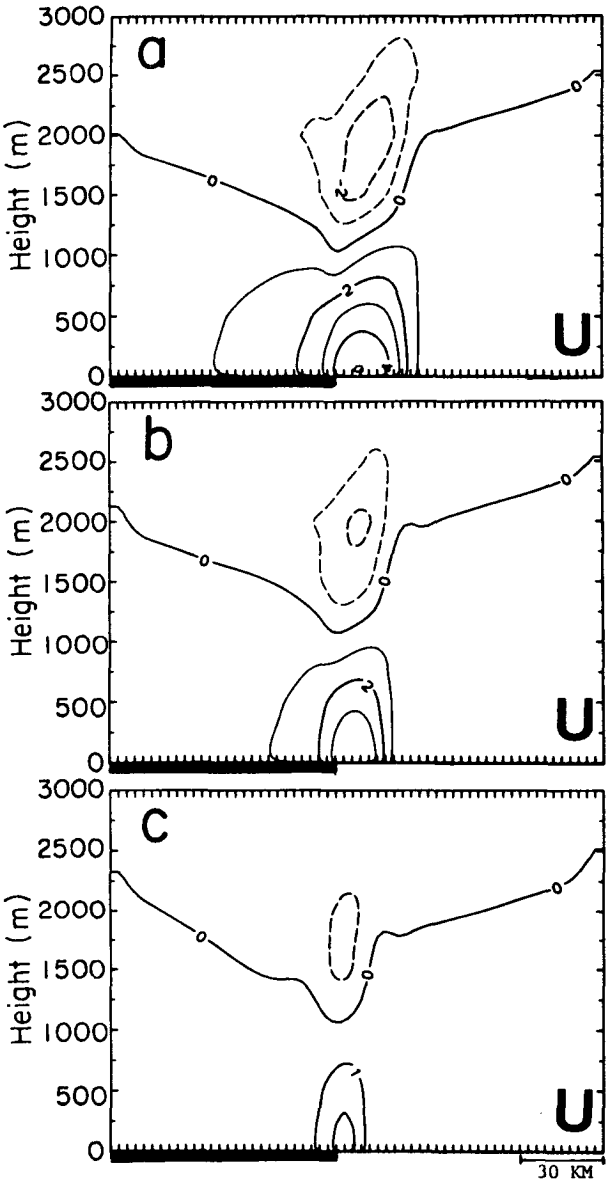

FIG. 9. Simulated snow-breeze u component (m s^{-1}) for case SB7 with (a) $f = 0.25$, (b) $f = 0.5$, and (c) $f = 0.75$.

bilization of the surface layer compared to the previous case (Fig. 11b).

Figure 12 (Case SL3) provides an illustration of the 21 March situation for the daytime, while Fig. 13 (Case SL4) provides an illustration of the development of the downslope flow under the same slope conditions as in Case SL3, except for nocturnal conditions (the simulation started at 1800 LST for case SL4). Comparing Figs. 12 and 13, the drainage flow at night is noticeably more intense and the thermal stabilization of the surface layer is much larger than the daytime snow-cover case. Obviously, the thermal energy contribution, through solar radiation, to the upper snow layer leads to an increased daytime snow surface temperature compared to the nocturnal period and, therefore, a less pronounced surface inversion. For contrast purposes, Case SL3 was rerun with snow-free ground (Fig. 14, Case SL5). An upslope flow component of over 2 m s^{-1} is found (Fig. 14a) with a small v component (Fig. 14b), and with a noticeable convective ABL related to the increased surface sensible heat fluxes (Fig. 14c).

The simulated u component for 21 December for an 800 m high plateau with snow cover (Case SL6) is presented in Fig. 15a. Intensification of the daytime drainage flow as compared to that for the shallow slope (SL1) is evident. A less pronounced change is simulated for the same terrain in the 21 March case (Case SL7, Fig. 15b). Repetition of SL7, however, with $z_0 = 0.5$ m (i.e., assuming a forest canopy covered entirely by snow) indicate some reduction in the downslope flow due to increased frictional effects (Case SL8, Fig. 15c).

It frequently occurs that snow cover is found over elevated terrain while the lower terrain is snow free. SL9 provides an illustration of such a situation during early spring, where the terrain above 400 m was assumed to be snow covered. Qualitatively the mesoscale flow features are associated with (i) upslope flow over the lower portion of the slope; (ii) thermally induced drainage flow over the snow-covered upper portion; and (iii) a slope snow breeze, due to the ABL thermal contrast along the slope. Based on our knowledge relating to the magnitude of the thermal forcing associated with (i) and (iii), and as seen in previous simulations, these forcings are likely to be more significant than those associated with (ii). Figure 16a illustrates the flow pattern for this simulation, with the snow breeze reaching a peak of $\approx$6 m s^{-1} and being more pronounced than the upslope flow. The coupling of the slope snow breeze and the upslope flow generates a noticeable convergence zone along the lower slope (Fig. 16b). The differentiation of the ABL characteristics between the snow-covered area and the snow-

TABLE 5. Brief description of the slope simulations (slope angle; date, surface conditions).

Simulation	Description	Figure
SL1	$\alpha = 0.382°$, 21 December, snow cover	10
SL2	$\alpha = 0.382°$, 21 December, snow cover, cold air	11
SL3	$\alpha = 0.382°$, 21 March, snow cover	12
SL4	$\alpha = 0.382°$, 21 March, snow cover, night	13
SL5	$\alpha = 0.382°$, 21 March, snow-free ground	14
SL6	$\alpha = 0.764°$, 21 December, snow cover	15a
SL7	$\alpha = 0.764°$, 21 March, snow cover	15b
SL8	$\alpha = 0.764°$, 21 March, snow cover, $z_o = 0.5$ m	15c
SL9	$\alpha = 0.764°$, 21 March, half upper domain snow covered	16
SL10	$\alpha = 0.764°$, 21 March, elevated terrain is snow covered	17
SL11	$\alpha = 0.764°$, 21 December, with $f = 0.1$	18a
SL12	$\alpha = 0.764°$, 21 March, with $f = 0.1$	18b

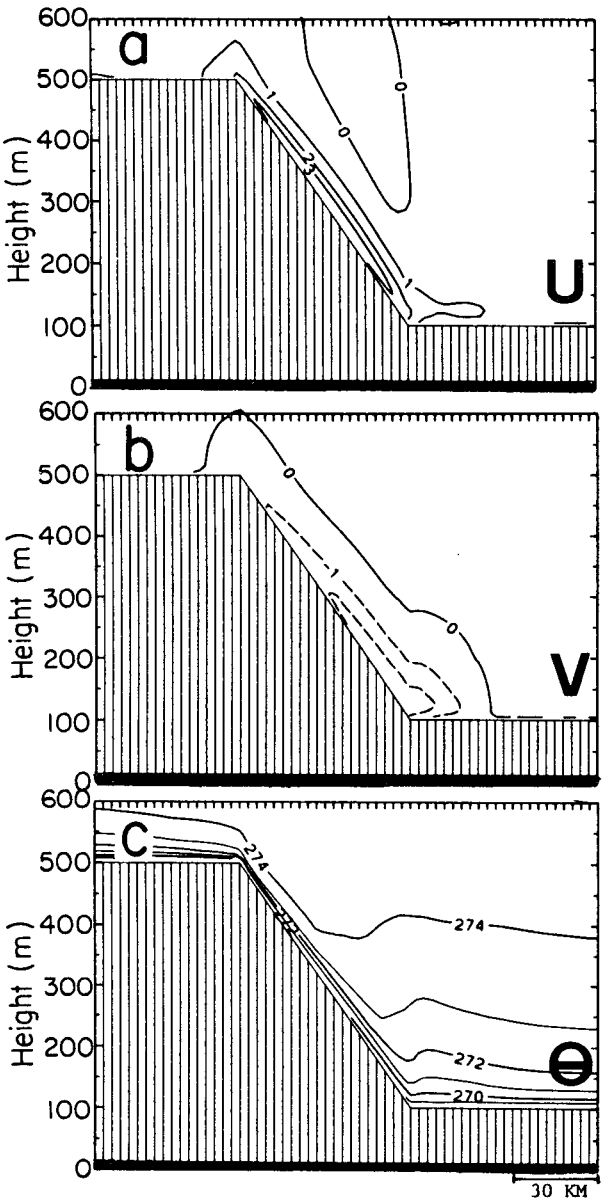

FIG. 10. Simulated thermally induced slope flow features at 1400 LST, in the domain vertical cross section for case SL1; (a) u component (m s^{-1}) (positive values—downslope flow component, solid contours; negative values—upslope flow component, dashed contours); (b) v component (m s^{-1}); and (c) potential temperature, θ (K).

free area is evident in Fig. 16c through the potential temperature field. The contrast in thermal structure resembles that simulated in the snow-breeze case (see Fig. 6d).

Ookouchi et al. (1984) simulated a situation similar to SL9, except the snow-covered area is replaced by wet ground. As implied from that study, well-defined relations can be established between the slope angle (a decrease in slope angle tends to emphasize the slope breeze), the thermal contrast within the ABL along the slope (its increase tends to intensify the slope snow breeze), and the initial potential temperature lapse rates (its increase tends to suppress the slope snow breeze) [see Ookouchi et al. 1984; Eqs. (15)–(16), p. 2290]. These relations can also be applied for the specific evaluation of slope-snow breeze.

Figure 17 illustrates salient features of Case SL10. The retreat of the snow cover to the plateau sections enabled the development of stronger upslope flows than in the previous case. The coupling of the snow breeze and the upslope flows leads to a noticeable convergence zone at the upper slope (Fig. 17b) associated with a sharp horizontal temperature gradient (Fig. 17c).

Figure 18 illustrates the impact of uniform bare ground patches within the snow area which cover 10% of the area ($f = 0.1$), for (a) 21 December and (b) 21 March. In each case the contribution of sensible heat flux from these patches is sufficient to induce a weak daytime upslope flow. When values of $f \lesssim 0.1$ were introduced, suppression of the upslope flows and an initiation of downslope induced flows were simulated. Note the more developed upslope flow on 21 March,

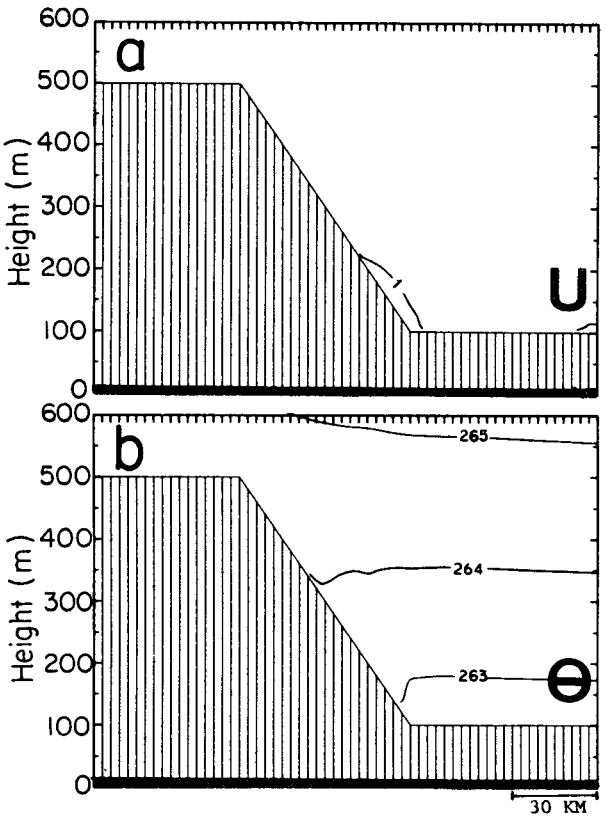

FIG. 11. Simulated thermally induced slope flow features in the domain vertical cross section for case SL2. (a) u component (m s^{-1}) and (b) potential temperature, θ (K).

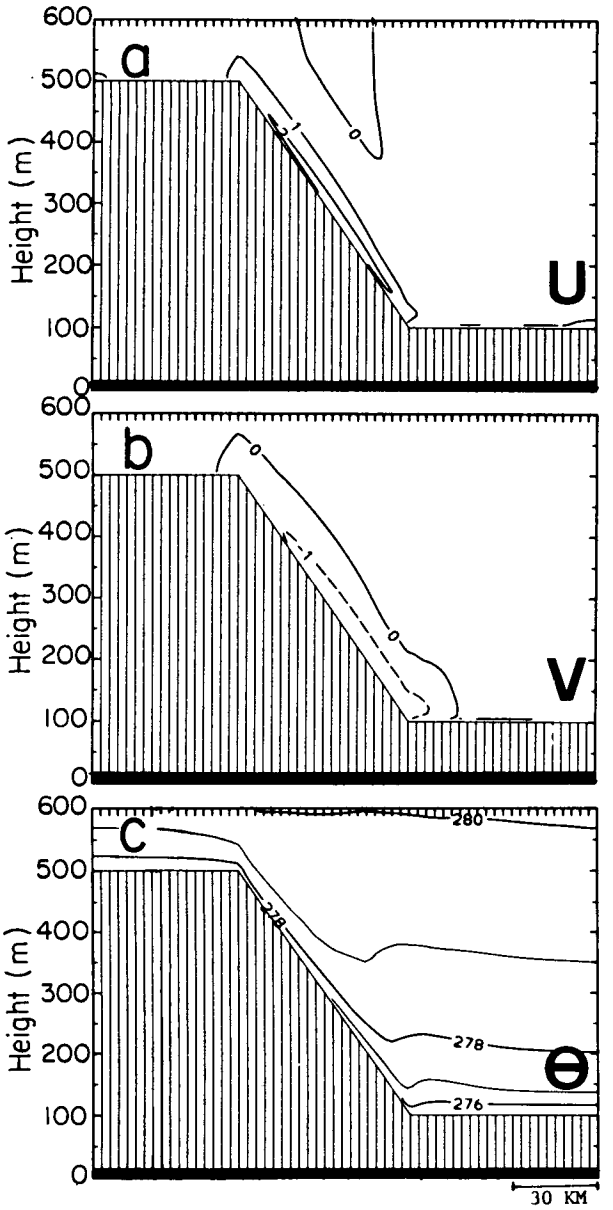

FIG. 12. Simulated thermally induced slope flow features in the domain vertical cross section for case SL3. (a) u component (m s^{-1}); (b) v component (m s^{-1}); and (c) potential temperature, θ (K).

due to the increased sensible heat flux from the bare ground.

6. Discussion

A numerical mesoscale model with a snow-layer module, together with conceptual and scaling arguments, have been used to evaluate the impact of an extensive snow cover on the generation of snow breezes, as well as on the modification of the daytime thermally induced slope flows.

In warm weather conditions (i.e., $T_a > 273$ K) a mesoscale region having a uniform and full cover of snow can be interpreted conceptually as a cold lake, so that snow breezes, in analogy to the lake breeze, should be generated. In this situation the *depth of the snow and its albedo are* not relevant, since the snow-surface temperature is constrained to be ≤273 K and

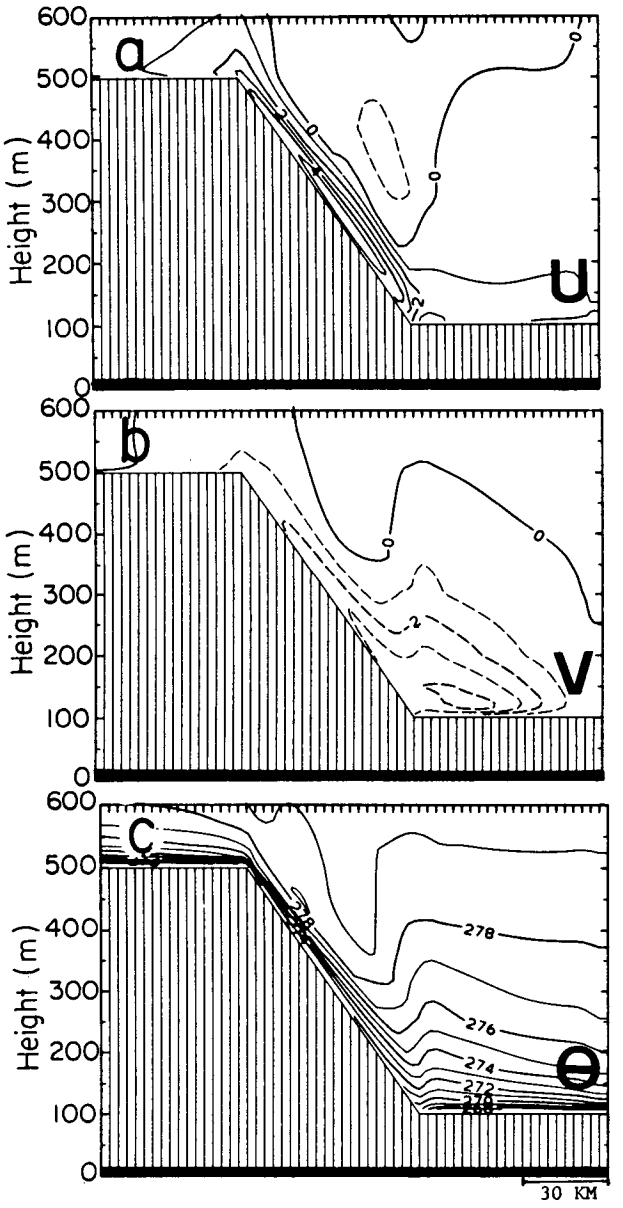

FIG. 13. Simulated thermally induced slope flow features, at 0200 LST, in the domain vertical cross section for SL4. (a) u component (m s^{-1}); (b) v component (m s^{-1}); and (c) potential temperature, θ (K).

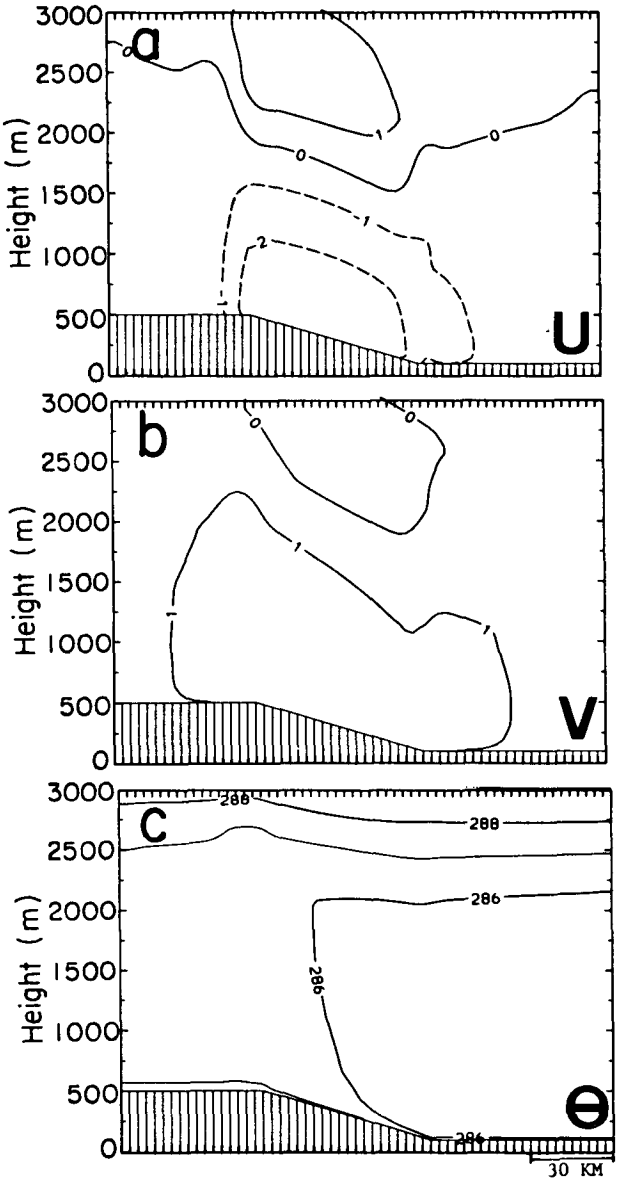

FIG. 14. Simulated thermally induced slope flow features in the domain vertical cross section for case SL5. (a) u component (m s^{-1}); (b) v component (m s^{-1}); and (c) potential temperature, θ (K).

it is the heating over adjacent bare ground area that is instrumental in producing a snow breeze. Any surplus of thermal energy in the snow will produce snow melt or modification of the thermal storage below the snow surface. A very *thin, uniform* snow cover, with a low albedo (e.g., snow that has been affected by dust/organic material deposition), will have the same effect on the generation of snow breezes as will deep and fresh snow cover. Therefore, the snow breeze is likely to be more pronounced in fall/early winter or late winter/spring situations, and in situations where snow cover exists in southerly latitudes. Worth noting, also, is that a canopy area covered completely by snow has nearly the same effect on the generation of a snow breeze, as does snow covered ground in the absence of canopy.

In many flat-terrain locations affected by snow cover, vegetation cover is likely to be low or absent in the winter (e.g., the cultivated areas in the U.S. Great Plains) and the likelihood of uniform snow cover free from bare ground patches or snow-free canopies is high. In any case, the sensible heat flux to the atmosphere

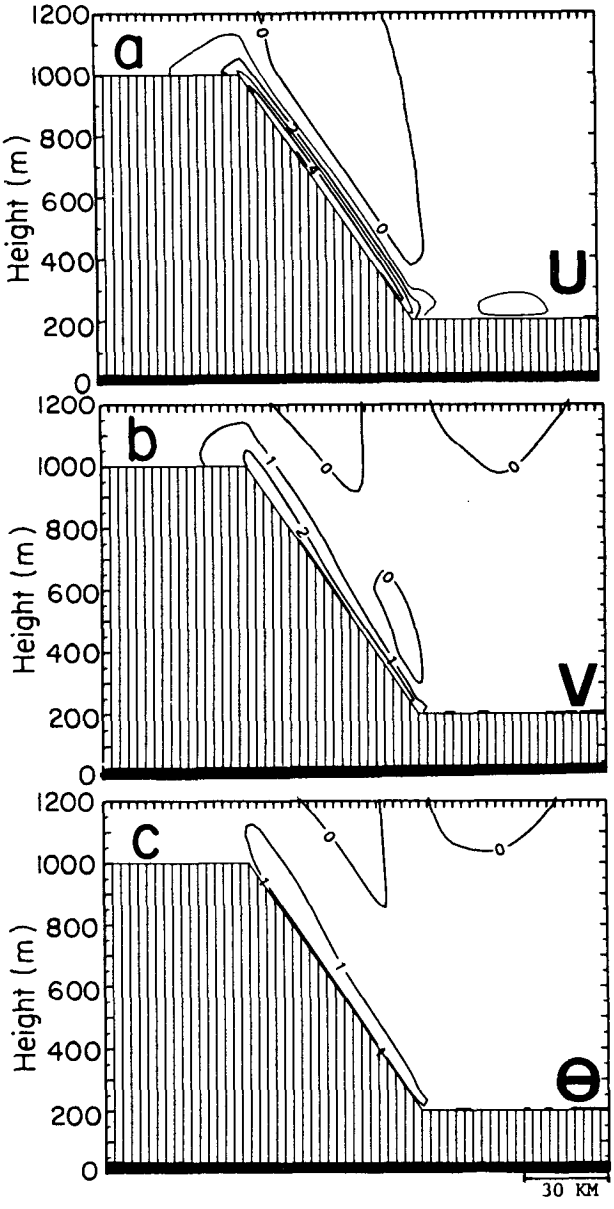

FIG. 15. Simulated u component (m s^{-1}) for (a) case SL6, (b) case SL7, and (c) case SL8.

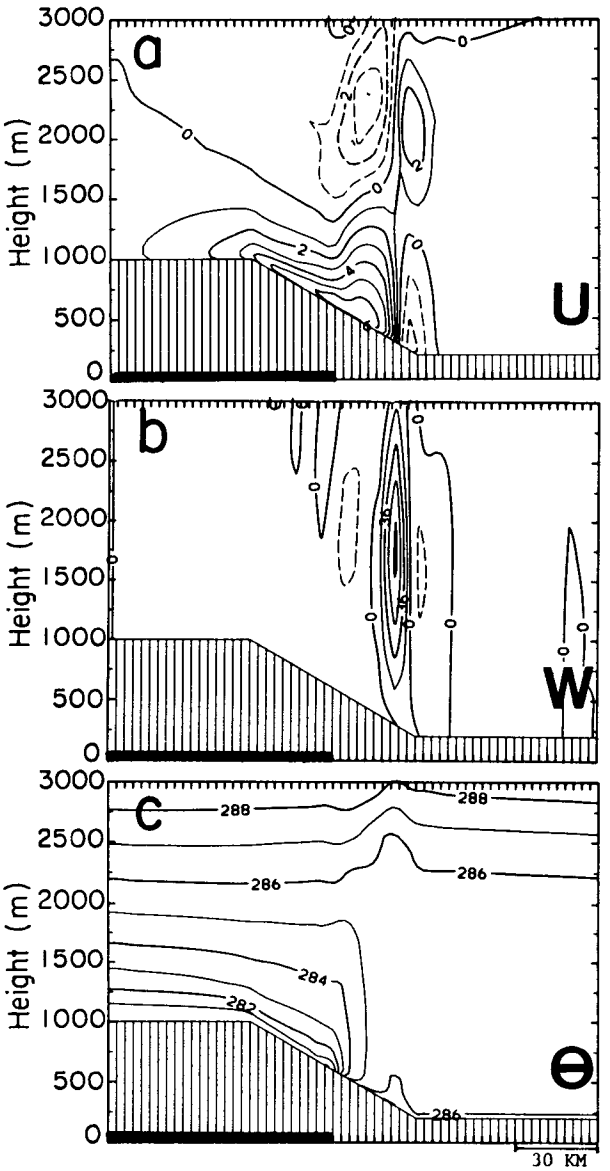

FIG. 16. The simulated thermally induced upslope flow features in the domain vertical cross section for Case SL9; (a) u component (m s^{-1}); (b) vertical velocity (cm s^{-1}); and (c) potential temperature, θ (K).

from the snow-free regions should contribute little to the areal heat flux so long as the fractional snow-free patchy area is small ($\leqslant 0.10$). Any further increase in this fractional area will result in a reduction in the intensity of the snow breeze.

The impact of uniform snow cover on the daytime thermally induced slope flow is determined by the associated modifications to the sensible heat and the longwave radiation flux divergence in the lower atmosphere. The daytime surface sensible heat fluxes over uniform snow cover tend to be much smaller (and usually in midwinter with a reversed sign) than that over snow-free surfaces under the same environmental conditions. In most cases, and specifically when the background air temperature is >273 K, a stable thermal stratification commonly prevails with negative surface sensible heat fluxes. Model sensitivity simulations gave small positive heat fluxes (i.e., to the atmosphere) over snow when a cold atmosphere is imposed on a snow surface with an initial $T \approx 273$ K. The magnitude of the sensible heat fluxes over the snow depends on parameters such as surface roughness, snow albedo and wind speed. The contribution of the longwave flux di-

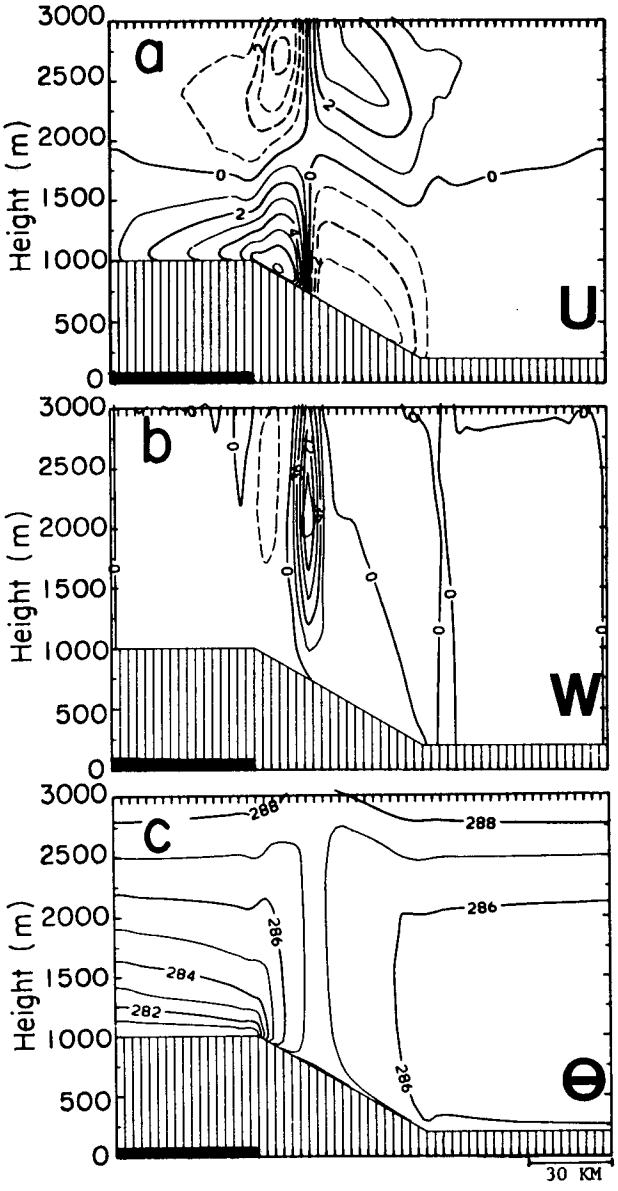

FIG. 17. The same as Fig. 16, except for case SL10.

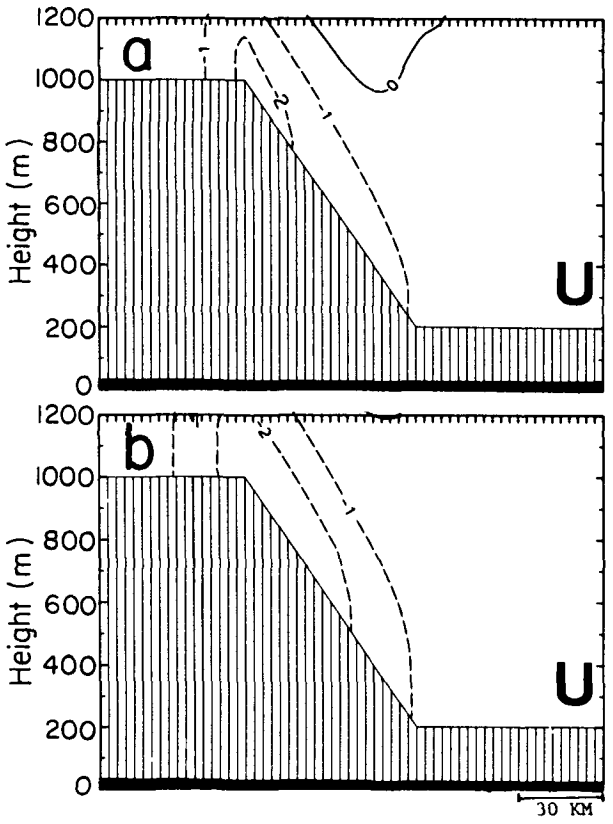

FIG. 18. Simulated u component (m s^{-1}) for (a) case SL11 and for (b) case SL12.

vergence to cooling/heating of the lower atmosphere over snow cover was suggested to be, at most, comparable to that from the divergence of the sensible heat flux.

Daytime drainage flows were simulated over uniform snow cover, although with intensities less than those found in nocturnal drainage flows. Since the magnitude of the negative sensible heat fluxes over snow cover is small (as well as the cooling contribution by the longwave flux divergence), even a small fraction of snow-free surface (i.e., canopy or bare ground) which is spread uniformly within the snow-covered area may offset the thermal forcing of the daytime drainage flow—this fraction was estimated at 0.1 (or even less). When the distribution of the bare ground patches within the snow area is less uniform, a larger area fraction of their coverage will likely be needed to totally eliminate the drainage flow. Vegetated slopes are typical in many mid-latitude mountainous areas, and suppression of the daytime upslope flow following snowfall over a densely forested slope is likely only for the period during which the *canopy is fully covered by snow*. When the snow is partially melted, or deposited on the ground below the canopy, the redevelopment of an upslope flow is likely.

Development of daytime convective cloudiness along mountainous slopes is common as spring approaches, so that convergence associated with the snowline retreat, and resulting from the coupling of the snow breeze and the thermally induced upslope flows, may well provide enhancement of convective cloud formation. However, on many occasions, this effect will be reduced by the presence of open canopies in the snow-covered area.

Acknowledgments. The study was supported by NSF grants ATM-8616662 and ATM-8915265 and EPRI Contract RP-1630-53. The model simulations were carried out at the NCAR computer center. Comments by an anonymous reviewer helped in improving the manuscript. B. Critchfield and D. McDonald prepared the manuscript.

REFERENCES

Anderson, E. A., 1976: A point energy and mass balance model of a snow cover. NOAA Tech. Rep. NWS 19, National Weather Service, 150 pp.

Arritt, R. W., 1987: The effect of water surface temperature on lake breezes and thermal internal boundary layers. *Bound.-Layer Meteor.*, **40**, 101–125.

Atwater, M. A., and J. T. Ball, 1978: A numerical solar radiation model based on standard meteorological observations. *Sol. Energy*, **21**, 163–170.

Bluestein, H. B., 1982: A wintertime mesoscale cold front in the southern plains. *Bull. Amer. Meteor. Soc.*, **63**, 178–185.

Chamberlain, A. C., 1983: Roughness length over sea, sand and snow. *Bound.-Layer Meteor.*, **25**, 405–409.

Charnock, H., 1955: Wind stress on a water surface. *Quart. J. Roy. Meteor. Soc.*, **81**, 639–640.

Cramer, J., 1988: Observational evaluation of snow cover effects on the generation and modification of mesoscale circulations. Paper No. 439, Department of Atmospheric Science, Colorado State University, Fort Collins, CO, 144 pp.

Dickinson, R. E., A. Henderson-Sellers, P. J. Kennedy and M. F. Wilson, 1986: Biosphere–atmosphere transfer scheme (BATS) for the NCAR community climate model. NCAR Tech. Note 275, NCAR, Boulder, CO, 69 pp.

Estoque, M. A., 1962: The sea breeze as a function of the prevailing synoptic situation. *J. Atmos. Sci.*, **19**, 244–250.

Estournel, C., R. Vehil and D. Vedalia, 1986: An observational study of radiative and turbulent cooling in nocturnal boundary layer (ECLATS Experiment). *Bound.-Layer Meteor.*, **34**, 55–62.

Garratt, J. R., and R. A. Brost, 1981: Radiative cooling effects within and above the nocturnal boundary layer. *J. Atmos. Sci.*, **38**, 2730–2746.

Granger, R. J., and D. H. Male, 1978: Melting of a prairie snowpack. *J. Appl. Meteor.*, **17**, 1833–1842.

Gray, D. M., and A. D. J. O'Neil, 1974: Application of the energy budget for predicting snowmelt runoff. *Advanced Concepts and Techniques in the Study of Snow and Ice Resources*, H. S. Santeford, and J. L. Smith, Eds., Nat. Acad. of Sci., Washington, DC., 108–118, [ISBN 0-309-02235-5].

Halberstam, I. M., and R. Melendez, 1979: A model over the planetary boundary layer over snow surface. *Bound.-Layer Meteor.*, **16**, 431–452.

Hicks, B. B., 1981: An analysis of Wangara micrometeorology: Surface stress, sensible heat, evaporation, and dewfall. NOAA Tech. Memo. ERL ARL-104, 36 pp.

——, and H. C. Martin, 1972: Atmospheric turbulent fluxes over snow. *Bound.-Layer Meteor.*, **2,** 496–502.

Kondo, T., 1975: Air sea bulk transfer coefficients in diabatic conditions. *Bound.-Layer Meteor.*, **9,** 91–112.

Joffre, S. M., 1982: Momentum and heat transfers in surface layer over frozen sea. *Bound.-Layer Meteor.*, **24,** 211–229.

Johnson, R. H., G. S. Young, J. J. Toth and R. M. Zehr, 1984: Mesoscale weather effects of variable snow cover over northeast Colorado. *Mon. Wea. Rev.*, **112,** 1141–1152.

Mahrer, Y., and R. A. Pielke, 1977: A numerical study of the air flow over irregular terrain. *Contrib. Atmos. Phys.*, **50,** 98–113.

——, and M. Segal, 1979: Simulation of advective Sharav conditions over Israel. *Isr. J. Earth Sci.*, **28,** 103–106.

Manins, P. C., and B. L. Sawford, 1979: Katabatic winds: A field case study. *Quart. J. Roy. Meteor. Soc.*, **105,** 1011–1025.

McCumber, M. C., 1980: A numerical simulation of the influence of heat and moisture fluxes upon mesoscale circulation. Ph.D. thesis, University of Virginia, 255 pp.

McKay, D. C., and G. W. Thurtell, 1978: Measurements of the energy fluxes involved in the energy budget of snow cover. *J. Appl. Meteor.*, **17,** 339–349.

McNider, R. T., and R. A. Pielke, 1981: Diurnal boundary development over sloping terrain. *J. Atmos. Sci.*, **38,** 2198–2212.

Mellor, M., 1977: Engineering properties of snow. *J. Glaciol.*, **19,** 15–66.

Monteith, J. L., Ed., 1976: *Vegetation and the Atmosphere, Vol. 2.* Academic Press, 439 pp.

Ohata, T. K., K. Higuchi and K. Ikegami, 1981: Mountain–valley wind system in the Khumbu Himal, East Nepal. *J. Meteor. Soc. Japan,* **59,** 753–762.

Oke, T. R., 1987: *Boundary Layer Climates.* Methuen, 372 pp.

Ookouchi, Y., M. Segal, R. C. Kessler and R. A. Pielke, 1984: Evaluation of soil moisture effects on the generation and modification of mesoscale circulations. *Mon. Wea. Rev.*, **112,** 2281–2292.

Schlatter, T. N., 1972: The local surface energy balance and subsurface temperature regime in Antarctia. *J. Appl. Meteor.*, **11,** 1048–1062.

——, V. D. Barker and J. F. Henz, 1983: Profiling Colorado's Christmas Eve blizzard. *Weatherwise,* **36,** 60–66.

Segal, M., and R. A. Pielke, 1985: On the effect of water temperature and synoptic flows on the development of surface flows over narrow elongated water bodies. *J. Geophys. Res.*, **90,** 4907–4910.

——, R. Avissar, M. C. McCumber and R. A. Pielke, 1988a: Evaluation of vegetation effects on the generation and modification of mesoscale circulations. *J. Atmos. Sci.*, **45,** 2268–2292.

——, R. A. Pielke, Jr. and Y. Ookouchi, 1988b: On optimizing solar collectors under daily non-random cloudiness conditions. *J. Sol. Energy. Eng.*, **110,** 346–348.

——, J. R. Garratt, G. Kallos and R. A. Pielke, 1989: On the impact of wet soil surface temperature and canopy temperature on the daytime development of the boundary layer. *J. Atmos. Sci.*, **46,** 3673–3684.

——, J. H. Cramer, R. A. Pielke, J. R. Garratt and P. Hildebrand, 1990: Observational evaluation of the snow-breeze. *Mon. Wea. Rev.*, **119,** 412–424.

——, J. R. Garratt, R. A. Pielke, P. Hildebrand, F. A. Rogers, J. Cramer and A. Schanot, 1991b: On the impact of snow cover on daytime pollution dispersion. *Atmos. Environ.*, **24B,** in press.

Tabler, R. D., 1980: Self similarity of wind profiles in blowing snow allows outdoor modeling. *J. Glaciol.*, **26,** 421–434.

Washington, W. H., and C. L. Parkinson, 1986: *An Introduction to Three-Dimensional Climatic Modeling.* University Science Books, 422 pp.

Wiscombe, W. J., and S. G. Warren, 1980: A model for spectral albedo of snow. I: Pure snow. *J. Atmos. Sci.*, **37,** 2712–2733.

Ye, Z. J., M. Segal, J. R. Garratt and R. A. Pielke, 1989: On the impact of cloudiness on the characteristics of nocturnal downslope flows. *Bound.-Layer Meteor.*, **49,** 23–51.

Yen, Y.-C, 1981: Review of thermal properties of snow, ice and sea ice. Rep. 81-10, U.S. Army, Cold Regions Research and Engineering Laboratory, Hanover, N.H., 34 pp.